Kinetics of cluster formation in the laser vaporization source: Carbon clusters

J. Bernholc and J. C. Phillips

Citation: The Journal of Chemical Physics **85**, 3258 (1986); doi: 10.1063/1.450996
View online: http://dx.doi.org/10.1063/1.450996
View Table of Contents: http://scitation.aip.org/content/aip/journal/jcp/85/6?ver=pdfcov
Published by the AIP Publishing

Kinetics of cluster formation in the laser vaporization source: Carbon clusters

J. Bernholc[a)]
Corporate Research Science Laboratories, Exxon Research and Engineering Company, Annandale, New Jersey 08801

J. C. Phillips
AT&T Bell Laboratories, Murray Hill, New Jersey 07974

(Received 24 March 1986; accepted 3 June 1986)

A general model of cluster formation in the laser vaporization source starting from the atomic vapor is developed and applied to carbon clusters. Two limiting cases of cluster growth exist: the diffusion-limited regime, in which the cluster distribution is essentially featureless, and the reaction-limited regime, in which the most stable clusters show as magic numbers in the cluster distribution. An approximate theory of the aggregation kernel allows for calculation of the cluster distribution in the reaction-limited regime from the formation energies of the reacting clusters. Heat released in cluster fusion allows small and medium size clusters to attain their lowest or almost lowest energy configurations in both the diffusion- and reaction-limited regimes. For larger clusters, crystalline structures are expected for transition metals, while network-forming materials are likely to exhibit a multitude of structures. An application to carbon clusters in the $n = 1$–25 range reproduce the experimentally observed cluster distributions and the magic numbers in the $n = 10$–25 regime. The equilibrium structures of the small carbon clusters formed in the nozzle are found to be chains and monocyclic rings. At the reaction temperature, the transition between the chain and ring structures occurs around $n = 10$ for the neutral and the positively charged clusters.

I. INTRODUCTION

The advent of the laser vaporization source[1–3] has made possible studies of clusters of almost any material and has revolutionized the cluster field. The first work dealt with diatomics, but the focus has quickly shifted to larger clusters.[4] Further improvements in the design of apparatus has allowed for the measurements of cluster distribution up to 100 atoms,[4] of cluster reactivity[5,6] and its connection to the photoionization threshold,[7] of photofragmentation pathways,[8,9] of positive and negative clusters formed directly in the source,[10] and of electron affinities.[11] A somewhat different apparatus has been used for extensive studies of the reactivity of iron clusters,[12] although the basic operational principle remains the same. The ease with which clusters in a wide range of sizes are made in the laser vaporization source once the design and testing of the machine has been completed has spurred further growth in this area. To date, cluster abundance spectra have been measured for many of the elements,[13] and work on compound materials has also started to appear.[14]

The interest in clusters stems from many sources. The clusters of various sizes offer comparisons between molecular and bulk properties. In the past, clusters of small to moderately large sizes have often been used to model bulk materials and their surfaces. Employing the newly developed experimental techniques, the transition from cluster to bulk behavior and the transition from cluster surfaces to bulk surfaces can now be studied experimentally. For example, the measurements of photoionization thresholds for carbon clusters show a slow convergence to the bulk work function.[4]

Modifications of the original design[5,6,12] of the cluster source allow for the studies of reactivity directly in the cluster beam. The observed reactivity patterns are often very unusual, like the direct insertion of a metal atom into a C–H bond.[15] For charged clusters, which can be mass-selected, photofragmentation[8,9] and reactivity studies can be performed on single size ions.

For covalently bonded materials, the theory of network glasses[16] has predicted the existence of a critical cluster size, above which it is very difficult to satisfy all the bond length and bond angle constraints of the network short of assuming a high symmetry crystalline structure. This theory predicts the existence of defects and/or internal surfaces above the critical size of the cluster. Some of the predictions of this theory can now be tested experimentally.

The principal result from a cluster experiment is the abundance spectrum of positive or negative cluster ions as a function of cluster size. For many substances, the abundance spectra show local maxima at certain "magic" cluster sizes. These magic numbers are in some cases independent of the method by which the ions were obtained, e.g., the magic numbers for positive carbon ions in the $n = 10$–25 range are the same for clusters made by laser vaporization of a carbon foil in vacuum[17] and for clusters made in the laser vaporization source where clusters are formed in the presence of a He carrier gas.[4,10] Furthermore, the charged clusters formed directly in the carrier gas[10] have the same magic numbers as charged clusters obtained by photoionization of neutral species.[4]

To date, magic numbers have been seen in cluster experiments for molecules,[18] noble gases,[19] alkali metals,[20] and semiconductors.[4,8,13,21,22] For transition metals, no magic numbers are observed in the cluster abundance spectra, but

a) Present address: Department of Physics, North Carolina State University, Box 8202, Raleigh, NC 27695.

 0021-9606/86/183258-10$02.10

significant structure exists in the reactivity data as a function of cluster size.[5,7] This structure correlates well with the variation in photoionization threshold as a function of cluster size.[7]

The magic numbers are usually interpreted as corresponding to clusters more stable than other clusters of similar size. For a few classes of materials, the principles determining cluster stability and the occurrence of magic numbers have been identified and many magic numbers have been predicted theoretically. For noble gases, which interact via van der Waals forces, geometric hard sphere packing determines the structures of the magic clusters. Since icosahedral packing is denser than close-packed structures up to several thousand atoms,[23] the magic numbers for the noble gas clusters are the Mackay icosahedral structures at 13, 19, 55, 147, etc. The experiments detect charged clusters, however, and it has been shown that ionization-induced fragmentation significantly affects the spectra of noble gas clusters.[24–26]

For the free-electron-like alkali metals, a good description of the bonding is provided by a spherical jellium model.[20,27] In this model, the electrons fill the one-electron levels corresponding to the self-consistent jellium potential which can be approximated for the purposes of identifying the magic numbers by a spherical square well potential. The additional stability of the magic clusters comes from a complete filling of a set of one-electron levels. The clusters with only partially filled HOMO are less stable, by analogy to the closed and open shell atoms in the Periodic Table. Later work,[28] has shown that ellipsoidal distortions of the alkali metal clusters can weaken some of the peaks predicted by the spherical jellium model. The major magic numbers for the alkali clusters are predicted to occur at 2, 8, 20, 40, etc.,—in good agreement with the experimental data.

For partially ionic compound materials, the Coulomb interactions between the cations and anions can determine the structure of the magic clusters. With help of a point charge ionic model, Martin and co-workers[29] predicted the structures of several magic clusters of partially ionic materials.

The theoretical effort aimed at explaining the cluster distribution spectra obtained in the laser vaporization source has generally focused on the thermodynamic aspects of the cluster formation and on cluster stability. Hagena,[30] Soler *et al.*[31] and Soler and Garcia,[32] on the other hand, have carried out kinetic calculations of the distribution of large molecular clusters. In their case, the clusters were made by thermal expansion of the molecules in vacuum without the presence of a carrier gas. The aggregation proceeded by bimolecular collisions with a constant sticking coefficient. Since the calculations are purely classical, no magic numbers are present and only the overall shape of the cluster distribution is obtained.

In this work, we analyze the cluster formation process in the laser vaporization source, present a general mean-field kinetic model of cluster aggregation, and apply it to carbon clusters. The model developed here is tractable enough to enable relatively simple calculations of the cluster distribution spectra. Two limiting cases of the cluster growth are discussed: One leads to the presence of magic numbers while the other does not, although the thermodynamic stability of clusters may show variations with cluster size in both cases. The kinetic analysis in Sec. II discusses the relative importance of the thermodynamic and kinetic effects. Section III describes the application of the kinetic model developed in Sec. II to carbon clusters. A number of results contained in this section were summarized previously.[33] Section III A reviews the experimental results. The next subsection discusses the structural models and gives the results of electronic structure calculations for clusters in the $n = 1$–25 range. Section III C presents the results of kinetic modeling of the experimental abundance spectra of positive, negative, and neutral carbon clusters. Section IV contains summary and conclusions.

II. KINETICS OF CLUSTER FORMATION

A. General considerations

A schematic diagram of the laser vaporization source is shown in Fig. 1. It consists of nozzle, an optional reaction tube, an expansion chamber, and a mass analyzer. A target material, located just below the nozzle, is vaporized by a pulsed laser. A pulsed stream of He carrier gas, synchronized with the vaporizing laser, carries the vapor down the nozzle towards the expansion chamber. During the passage through the nozzle, clusters grow by collisions among the vaporized particles. Collisions with He carrier gas provide cooling during growth. The cooled clusters are expanded and photoionized by a second laser. The resulting cluster distribution is measured in a mass analyzer. Low intensity spectra can also be obtained without the use of the photoionization laser, since the vaporization process generates a number of charged ions which collide with other clusters to produce a distribution of charged clusters. Optionally, a reactant gas can be injected into the reaction tube. The reactivity as a function of cluster size is measured as the loss of the original ion signal.

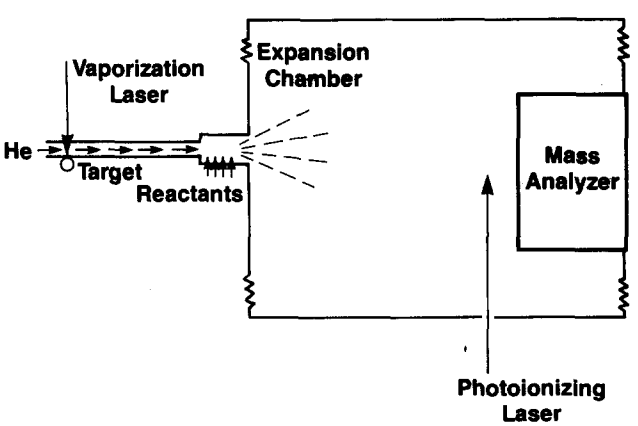

FIG. 1. A schematic diagram of the laser vaporization source. The vaporizing laser pulse is synchronized with a He pulse in the nozzle. The evaporated matter is carried by He towards the reaction chamber and the skimmer. Clusters formed in the nozzle are expanded, photoionized, and detected in a mass analyzer. Optionally, reactants are injected into the reaction chamber. The reactivity as a function of cluster size is measured as the loss of the bare cluster signal.

Since the short and intense laser vaporization pulse can raise the surface temperature of the target above the boiling temperature, the evaporated matter is generally assumed to be monoatomic.[34] Apart from general thermodynamic arguments, the support for this assumption comes from the large number of atoms and dimers detected by the mass analyzer[35] and from the variation of the cluster distribution as a function of He pressure. The ratio of charged to neutral atoms is very small because the atomic ionization energies are many times greater than the kinetic energies of the atoms even at the boiling temperature of the target (see also Ref. 36). However, good statistics can still be obtained in experiments which detect directly the charged clusters produced in the source,[10] because a photoionization step is not required.

Since He pressure in the nozzle ranges from 0.2 to several atmospheres, the atoms and clusters in the beam experience many He collisions between aggregation events. The aggregation proceeds thus by diffusion, with the diffusion coefficient determined by the He pressure and the cross section of the growing clusters. For a dilute solution of heavy particles in a light gas, the diffusion coefficient is[37]

$$D = (kT)^{3/2}/(\sigma p m_{\mathrm{He}}^{1/2}) , \quad (1)$$

where p is the partial pressure of He gas, σ is the cross section of the atom or cluster for collisions with He atoms, and m_{He} is the mass of the He atom. The expression (1) is valid for a gas, where the mean free path is much longer than the radius of the diffusing particle. In the opposite limit, i.e., for a macroscopic particle or in a liquid, the more familiar Stokes–Einstein relation is applicable[38] with the diffusion coefficient inversely proportional to the viscosity and the radius of the particle.

As is evident from Eq. (1), the lowering of the pressure of the carrier gas increases the number of collisions between the clusters. However, another important role of the carrier gas is the cooling of the growing clusters by He–cluster collisions. The need for cooling can be clearly seen by comparing bulk cohesive energies per atom with the average energies per atom at the melting temperature and at the boiling temperature for the same material. Such data are shown in Table I for representative alkali metals, semiconductors, and transition metals. Based on the data in Table I, one can make the qualitative conclusion that an addition of an atom to a cluster of the same material will raise the effective temperature of the cluster to above the boiling point for clusters smaller than 3 to 6 atoms, while an addition of an atom to a cluster smaller than 7 to 14 atoms will raise the effective temperature of the cluster above the melting point. However, since for a small cluster a large fraction of the total number of atoms resides on the surface, the melting or boiling of a cluster will occur at temperatures much lower than the corresponding bulk values. Indeed, Buffat and Borel[39(a)] have found that the melting temperature of gold clusters dropped from the bulk value of 1337 K to below 400 K for clusters smaller than 25 Å [see also Ref. 39(b)].

TABLE I. Representative values of cohesive energies E_c, melting point energy E_m, boiling point energy E_b, and the activation energy E_V^m for vacancy migration for alkali metals, semiconductors, and transition metals. All energies are in eV/atom or eV/defect.

	E_c	E_m	E_b	E_V^m
Na	1.13	0.096	0.30	
K	0.94	0.087	0.27	
C	7.36	0.99	1.3	
Si	4.64	0.44	0.68	0.3[a]
Cu	3.50	0.35	0.73	0.7[b]
Au	3.78	0.35	0.80	0.8[b]
Ni	4.44	0.32	0.78	1.3[c]
Pt	5.85	0.53	1.06	1.4[b]

[a] Reference 60.
[b] Reference 61.
[c] Reference 62.

Effective temperatures above the boiling point will lead to monomer evaporation. Data on alkali metal clusters[20] formed under a moderate pressure of Ar carrier gas in an apparatus of a different design than the one discussed in the present paper, show evidence of evaporation from clusters just above the magic numbers to the more stable magic clusters, since the abundance spectra exhibit strong depletions in the regions just above the magic numbers. The increase in the effective temperature may be due to insufficient cooling during the cluster growth time and to heating of the clusters during ionization.

Although the quantification of the above arguments would require detailed considerations of the experimental time scales, the effective cooling rates, and the nature of the particular ground and excited states, it is clear that lowering of the He pressure will impede the growth of clusters by lowering the cooling rate. The input He pressure thus has to stay within the well defined but equipment specific range for optimum cluster growth.

A structural rearrangement of a cluster can occur at temperatures well below its effective melting temperature. For example, rearrangements involving defect annealing require relatively little excess energy, since the activation energies for defect migration are usually small (see Table I). This argument suggests that below the size of 20–40 atoms and sometimes for even larger clusters one should expect either a single well-defined cluster structure or at most a few alternative structures, since the energy released in cluster fusion is sufficient for rearrangements to these structures. The uniqueness of the structures of smaller to medium size clusters explains the reproducibility of the size-dependent properties of these clusters, e.g., the size-dependent reactivity data.[5,6] For larger cluster sizes, the energy released in atom or cluster addition is insufficient to cause melting. Since the time scale of vibrations is of the order of 10^{-13} s, the extra energy is quickly redistributed throughout the cluster. Only limited "local" melting is thus possible before the redistribution takes place. Consequently, the larger clusters made by atom–cluster and cluster–cluster aggregation will have a distribution of structures and the experiments will measure the average properties of this distribution. The classical analogs of this situation are the diffusion limited aggregation model of Whitten and Sander,[40(a)] where clusters aggregate randomly with the sticking coefficient equal to unity, and the closely related "chemical aggregation" model,[40(b)] where the sticking coefficient is taken to be very small but independent of cluster size or structure.

The foregoing general arguments are subject to significant qualitative variations from one class of materials to another. For example, transition metals (such as Ni) tend to crystallize when deposited from the vapor even at substrate temperatures $T_d = 4$ K. Transition metal clusters deposited from vapor have been observed to have crystalline structures even at sizes of 400 or more atoms, e.g., gold[39(c)] and copper.[39(d)]. Network materials such as Si, on the other hand, may remain amorphous when deposited from the vapor at temperatures as high as $T_d/T_m \sim 0.3$ (500 K for Si). Finally, glass-forming materials such as SiO_2 are always noncrystalline when deposited from the vapor or rapidly quenched from the melt at temperatures below the glass transition temperature T_g, where values of T_g as high as $T_g/T_m = 0.8$ are typical for very good glass formers (such as SiO_2). This phenomenology, in turn, needs modification on a scale of cluster size of order 30–100 atoms, where crystalline order is now being resolved by high resolution transmission electron microscopy.[41]

The conclusion to be drawn from the preceding discussion is that for large or relatively simple clusters spheroidal shapes are expected for most materials. For clusters which assume crystalline structures, the termination surfaces will consist of crystal planes of low surface energy.[39(e)] However, for materials where the structure characteristically has a network form, with small average coordination numbers near three, much more complex behavior is possible because of the slowing of configurational relaxation which is the microscopic analog of glass formation in macroscopic solids. In this context we expect that graphite-based carbon microclusters may exhibit several exotic structures, and this expectation is realized experimentally.

B. Rate equations

The mean-field rate equations governing the aggregation of particles, due to Smoluchowski,[42] are

$$\dot{x}_i = \sum_{j=1}^{i-1} K_{ji-j} x_j x_{i-j} - \sum_{j=1}^{N} 2K_{ij} x_i x_j, \quad i = 1,...,N. \tag{2}$$

In Eq. (2) x_i denotes the concentration of clusters of size i. K_{ij}, the aggregation kernel, determines the time-dependent aggregation probability. The first term on the right-hand side of Eq. (2) describes the increase in the concentration of clusters of size i due to the fusion of two clusters of size j and $i-j$. The second term describes the depletion of clusters of size i due to the formation of larger clusters.

For applications to the laser vaporization source, Eqs. (2) must be generalized to include the neutral–positive, neutral–negative, and positive–negative cluster fusion because the vaporization process produces ions as well. The number of ions depends of course on the power and duration of the laser pulse. However, since the electrons and the ions are attracted by long-range Coulomb forces, the recombination processes are very fast, leading to a population of neutral atoms being much larger than that of the ions even at the beginning of the cluster growth process. For this reason, the probability for positive–negative cluster fusion is much smaller than that of neutral–positive and neutral–negative cluster fusion and can be neglected.

The terms due to the formation of positive clusters are

$$\dot{x}_i^0 = \dot{x}_i - \sum_{j=1}^{N} K_{ij}^{0+} x_i^0 x_j^+ \tag{3}$$

and

$$\dot{x}_i^+ = \sum_{j=1}^{i-1} K_{ji-j}^{0+} x_j^0 x_{i-j}^+ - \sum_{j=1}^{N} K_{ji}^{0+} x_j^0 x_i^+, \quad i = 1,...,N, \tag{4}$$

where $\dot{x}_i$ is defined by the right-hand side of Eq. (2) and $\dot{x}_i^0$ and $\dot{x}_i^+$ denote the concentration of the neutral and positively charged clusters, respectively. The kernels K_{ij} and K_{ij}^{0+} describe the neutral–neutral and neutral–positive aggregation probabilities. Analogous terms are introduced due to the presence of the negatively charged clusters.

During the cluster growth, there is also a possibility of charge transfer between the charged and the neutral clusters without the accompanying cluster fusion. The probability for electron transfer between the negatively charged and the neutral clusters is much greater than the probability of electron transfer between the neutral and the positively charged species, since electron affinities are much smaller than ionization potentials for small and medium size clusters. In our analysis of the carbon data (see Sec. III C), we found strong evidence for the occurrence of the former process, but none for the latter. We therefore include only the electron transfer terms from the negatively charged to the neutral clusters:

$$\dot{x}_i^0 = \dot{x}_i^0 - \sum_{j=1}^{N} T_{ij} x_i^0 x_j^- + \sum_{j=1}^{N} T_{ji} x_j^0 x_i^- \tag{5}$$

and

$$\dot{x}_i^- = \dot{x}_i^- + \sum_{j=1}^{N} T_{ij} x_i^0 x_j^- - \sum_{j=1}^{N} T_{ji} x_j^0 x_i^-, \tag{6}$$

where T_{ij} is the (nonsymmetric) charge transfer kernel. The coupled rate equations (3)–(6) are to be solved simultaneously for the concentrations of the neutral and the charged clusters.

Classically, the aggregation probability for clusters i and j with diffusion coefficients D_i and D_j is proportional to $D_{ij}R_{ij}$, where $D_{ij} = D_i + D_j$ is the joint diffusion coefficient for the two clusters, and R_{ij} is the "catching" radius within which the clusters will stick with unit probability.[42]

In a reactive aggregation, one has to consider the reaction probability within the interaction radius. The expression for reactive aggregation becomes

$$K_{ij} = 4\pi D_{ij} R_{ij} \frac{P_{ij}}{P_{ij} + P_D}, \tag{7}$$

where P_{ij} is the reaction probability per unit time and P_D is the probability of the reactants to diffuse away. One has $P_D = 1/\tau_{ij}$, where τ_{ij} is the average time in which the clusters remain within the reaction distance R_{ij}. From the diffusion equation one can easily show that $1/\tau_{ij} = 6D_{ij}/R_{ij}^2$ leading to the formula[43]

$$K_{ij} = 4\pi D_{ij} R_{ij} \frac{P_{ij}}{P_{ij} + 6D_{ij}/R_{ij}^2}. \tag{8}$$

The limiting forms of Eq. (8) are of particular interest. If $P_{ij} \gg P_D$, $K_{ij} \cong 4\pi D_{ij} R_{ij}$ and the distribution of cluster sizes is governed by the classical aggregation kinetics. No

reaction-induced magic numbers will arise in this case.[44] The shape of the cluster distribution will be featureless. The true solutions to Eqs. (2) can be approximated in this case by the ones corresponding to the exactly solvable simple kernels.[45] Since the variation of the kernels with cluster size is not very strong in the classical limit, a simple constant kernel solution[42]

$$x_i(t) = x_0 \frac{(Cx_0t)^{i-1}}{(1+Cx_0t)^{i+1}}, \tag{9}$$

where $K_{ij} = 2C$ and $x_1(t=0) = x_0$ may be used for qualitative purposes. A more accurate solution can be obtained numerically from Eqs. (3)–(6) provided one models the variation of the diffusion coefficients and the catching radia with cluster size. Since cluster reactivity varies with its structure, the uniqueness of the structure explains the reproducibility of the reactivity data[5,6] for small TM clusters.

A good example of cluster growth following classical kinetics is the formation of transition metal clusters, since the cluster distribution spectra of these materials are featureless.[13] It is important to point out, however, that although the distribution of transition metal clusters is classical, the small and medium size clusters will have unique or nearly unique shapes because of the heat released in cluster fusion (see Sec. II A).

In the other limit in Eq. (8), where $P_D = 6D_{ij}/R_{ij}^2 \gg P_{ij}$, the growth of clusters is *reaction limited*. In this case, one can neglect P_{ij} in the denominator of Eq. (8). The diffusion coefficients cancel, leading to the simple formula

$$K_{ij} \cong 4\pi/6R_{ij}^3 P_{ij} . \tag{10}$$

The aggregation probability in the *reaction-limited* regime is thus dependent only on the reaction probability and does not depend on the value of the diffusion coefficient. In this regime, the aggregating clusters will undergo several collisions before fusion. Since the reaction probabilities depend on the structure, symmetry, and stability of the reacting clusters, they are likely to show significant variations with cluster size. This is the regime in which magic numbers are observed.[44] The independence of the rate of fusion on the diffusion coefficient explains the reproducibility of the measured magic numbers under a wide variety of experimental conditions.

In order to calculate the cluster distribution in the reaction-limited regime, the knowledge of reaction probabilities for each pair of reacting clusters, including their charge dependence, is required. This is a prohibitive computational task at present and one is forced to make several approximations to make the calculations feasible.

In the simplest version of the transition state theory, the probability of the reaction is

$$P_{ij} = Ae^{-E^*/kT} \tag{11}$$

where the preexponential factor A is the product of the attempt frequency and the steric factor and E^* is the difference between the total energy of the activated complex in the transition state and total energy in the initial ground state. The calculation of the transition state energies for all possible pairs of reactants is, however, too big a task. Fortunately, the *relative differences* between transition state energies can be estimated from the Polanyi–Bronsted relationship. This relationship, long used in catalysis,[46] states that the lowering of the transition state energy in a reaction is proportional to its exothermicity, i.e.,

$$E^* = E_0 - \gamma(E_R - E_P) , \tag{12}$$

where E_0 is a constant part of the barrier, E_R and E_P are the total energies of the reactants and the products, respectively, and γ is the proportionality constant in the Polanyi–Bronsted relationship.

In cluster fusion, the reactants are likely to undergo substantial structural rearrangements after the initial attachment. The relation (12) is thus best used for the first step in the reaction. We define the scaled derivative

$$\Delta H_i' = n(\Delta H_{i+1} - \Delta H_i) , \tag{13}$$

where ΔH_i is the formation energy per atom of a cluster containing i atoms. This derivative describes the energy gain upon addition of a single atom. Assuming that the initial attachment proceeds via an interaction involving primarily two atoms, one on each cluster, the variation of the transition state energy with the size of the clusters can be approximated by

$$E_{ij} \cong E_0 + \gamma(\Delta H_i' + \Delta H_j') . \tag{14}$$

The final expression for the aggregation kernel is

$$K_{ij} = \alpha R_{ij}^3 e^{-\gamma(\Delta G_i' + \Delta G_j')/kT_{\rm av}}, \tag{15}$$

where the parameter α accounts for the concentration of the reactants, the preexponential factor and the constant part of the activation energy. The enthalpies in Eq. (14) have been replaced by Gibbs free energies in order to account for possibility of temperature-dependent structures due to the variation of cluster entropy with the structure. $T_{\rm av}$ denotes the average growth temperature.

In analogy to Eq. (15), the charge transfer kernel is approximated by

$$T_{ij} = \alpha R_{ij}^3 e^{-\xi(A_i + A_j)/kT_{\rm av}}, \tag{16}$$

where A_i denotes electron affinity of cluster i. Since the electronic wave function of a negatively charged cluster has a relatively large radius, the Polanyi–Bronsted proportionality factor ξ in the charge transfer kernel is significantly larger than the corresponding factor in the aggregation kernel.

Equations (15) and (16) require electronic structure calculations for only the end products, i.e., the stable neutral, positively and negatively charged clusters. Given the aggregation and charge transfer kernels, the coupled equations (3)–(6) are solved simultaneously for the concentrations of the neutral clusters and the ions. The quantities α, γ, and ξ are treated as adjustable parameters. The average temperature $T_{\rm av}$ is not known at the outset, but the analysis of experimental spectra provides an upper bound. The spectrum of positively charged clusters is thus determined by two adjustable parameters, while the negatively charged spectrum requires an additional parameter.

III. CARBON CLUSTERS

A. Experimental data

The early measurements[47] on pure carbon clusters date back to 1954. These experiments used a heated substrate as a

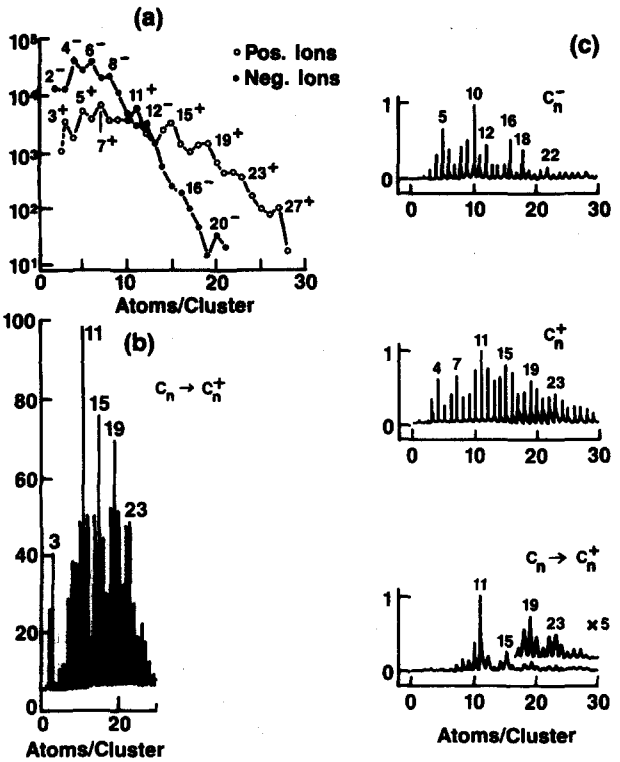

FIG. 2. Experimental abundance spectra of carbon clusters: (a) from Ref. 17; (b) from Ref. 4; and (c) from Ref. 10. The spectra labeled C_n^- and C_n^+ were obtained directly from the source. The label $C_n \rightarrow C_n^+$ indicates spectra obtained by photoionization of neutral clusters.

cluster source, while all later work used laser vaporization techniques. In the experiments of Fürstenau and Hillenkamp[17,48] a thin carbon foil was vaporized in vacuum with no carrier gas present, while the experiments of Cox, Rohlfing, and Kaldor[4] and of Bloomfield, Geusic, Freeman, and Brown[10] used the laser vaporization source. The results of the last three experiments are shown in Figs. 2(a)–2(c), respectively. The cluster distributions obtained directly from the source are labeled C_n^+ and C_n^-, respectively, while the distributions obtained by photoionization of neutral clusters are labeled $C_n \rightarrow C_n^+$. A comparison between the various spectra in Fig. 2 shows that the cluster distribution in the C_1–C_9 region depends strongly on the experimental conditions. For example, the magic numbers differ significantly between the photoionized spectra in Fig. 2(b) and in Fig. 2(c). In the C_{10}–C_{25} range, on the other hand, the magic numbers at 11, 15, 19, and 23 are identical for all the measurements on positive clusters, regardless whether they have been produced directly or a photoionization step was involved [cf. Figs. 2(a)–2(c)]. For negative clusters in the same range there is only partial agreement between the results of Ref. 17 and 10, i.e., the magic numbers are at 12, 16, and 20 in Fig. 2(a), but at 10, 12, 16, 18, and 22 in Fig. 2(b). This increased sensitivity to the particular experimental conditions may be due to the electron transfer effects (see below).

Above C_{25}–C_{30}, the intensity of the positive ions produced directly in the source decreases rapidly[10] and shows only weak magic number structure. This decrease is consistent with cluster production governed by aggregation kinetics. For ions produced by photoionization, the spectrum depends very strongly on the intensity of the vaporization laser[4(b),22], the entrainment time in the nozzle[4(b),22] and the wavelength and intensity of the ionizing laser.[4(b)] For example, ionization with a high intensity ArF laser ($h\nu = 6.42$ eV) results in a spectrum which exhibits a "dead" region between C_{30} and C_{38} [Ref. 4(a)]. Beyond C_{38} only even clusters are seen, and there is a broad maximum around C_{60}–C_{70}. Ionization with a low intensity F_2 laser ($h\nu = 7.87$ eV) results in a spectrum which has both even and odd peaks [Ref. 4(b)]. In both spectra C_{60} and C_{70} show as very strong "magic number" peaks. The structure of these large clusters has been plausibly identified in terms of spheroidal and ellipsoidal surface networks[22] of pentagons and hexagons which in the case of C_{60} is identical to that found on soccer balls. In this configuration each C atom has two single and one double bonds. It has been suggested[22] that these clusters have evolved from large fragments which were evaporated in graphitic structures by the original laser flash exposure of the graphitic source. The graphitic fragments attract each other by induced polarization (van der Waals-like forces), and the replacement of some hexagons by pentagons would occur during fusion as required to generate surface curvature and eventual cluster closure. The intensity of C_{60} and C_{70} peaks can be enhanced by increasing the vaporization laser power and increasing the entrainment time,[22] and also by increasing the ionizing laser intensity.[4(b)] The last effect shows that photofragmentation results in an increased concentration of C_{60}^+ and C_{70}^+. Recent calculations[49] for these and other polyhedra indicate that polyhedral structures become important at about C_{40} while graphitic structures may become important above C_{24}.

The formation of C_{60} and C_{70} clusters can be regarded as an intermediate step, similar to the formation of metastable phases in rapidly quenched melts, on the path to growth of microcluster C into bulk C phases. For the present analysis it appears that the three-dimensional structures become possible only beyond C_{40}, and are separate and distinct from the region C_1–C_{25} discussed here. As we shall see, it is likely that the first stage of closure (chain→ring) occurs near $n = 10$, while the second stage (layer→polyhedral surface) occurs near $n = 40$ (Ref. 49). Our aim is to show the kinetics in the first stage can be analyzed by the equations discussed in Sec. II.

B. Structure

A covalently bonded cluster will always attempt to minimize the number of dangling bonds. Among the elements, carbon is noted for its ability to form multiple bonds. The average bond strengths for single, double, and triple C–C bonds are[50] 83–85, 146–151, and 199–200 kcal/mol, respectively. By forming multiple bonds, the number of necessary dangling bonds can be reduced dramatically. The second and third bonds are not so strong as the first one, but for a finite system, if the alternative is an increased number of dangling bonds, the multiply bonded structures will prevail.

For the smallest clusters, the multiply bonded chain is obviously the structure containing the smallest number of dangling bonds, e.g., C_3 is linear, but no firm structures have been established for clusters larger than C_3 (see also Ref.

51). Bending of a chain into a ring removes the dangling bonds at the ends of the chain, but strain is introduced because the chain is *sp* bonded. The formation of a ring is thus favorable only for larger clusters. For yet larger aggregating clusters, fused rings and three-dimensional structures become reasonable possibilities, provided a low energy path exists from the fusing chains and rings to these structures.

For the smaller clusters, Pitzer and co-workers[52,53] have developed a π-electron model for neutral carbon chains and even-membered rings. They predict that neutral clusters form chains up to C_9 and rings for larger clusters. Hoffman's[54] extended Hückel calculations find the first ring to occur at C_{14}. Since the experiment measures the distribution of charged clusters, calculations for both charged and neutral clusters become necessary.

We have carried out self-consistent, geometry-optimized MNDO calculations[55] for neutral and charged chains and monocyclic rings up to $n = 25$. For the chains, the "inner" C–C distances were constrained to be equal, but could be different from the C–C distances involving an end atom. For the rings, all C–C distances were constrained to be equal.[56] For the neutral clusters, chains were found to be the preferred structures up to $n = 9$, with the odd-membered chains being more stable than the even ones. At $n = 10$, the monocyclic ring becomes somewhat more stable than the chain, while the chains are more stable for $n = 11$ and 12. The rings are more stable for yet larger systems. The formation energies per atom for the lowest energy structures for $n = 6$–25 are shown in Fig. 3(a). The particularly stable rings are at $n = 10$, 14, 18, and 22.

The regions of particular stability can be understood qualitatively by simple bonding considerations. In each of the clusters, the carbon atoms form one σ and one π bond to each of their neighbors. For the chains, there are $n - 1$ σ bonds and two dangling bonds, leaving $2(n - 1)$ electrons to occupy the π manifold. Since the π levels can hold four electrons each and clusters with fully occupied HOMO(s) are more stable, the odd-membered chains are preferred. For rings, the two π bonding planes (parallel and perpendicular to the ring) each have a nondegenerate (excluding spin), totally symmetric level as the lowest level, followed by doubly degenerate levels. Since every C atom contributes two π electrons, the most stable rings with the fully occupied HOMO are at $4n + 2$. This stability is in complete analogy to Hückel's rule for hydrocarbons, where the carbon atoms contribute one π electron each and π bonding occurs only in the plane perpendicular to the plane of the ring.

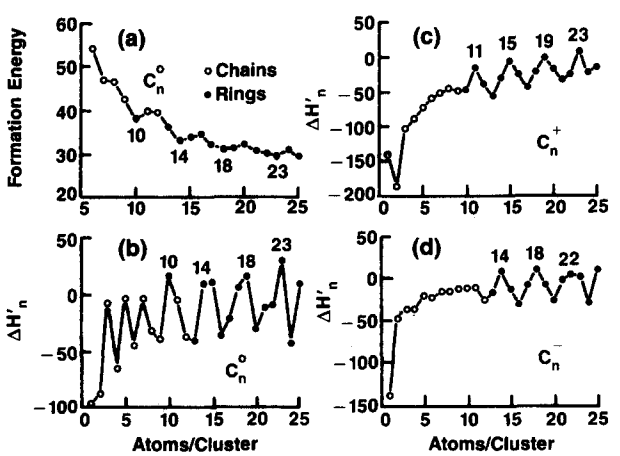

FIG. 3. (a) Formation energy/atom in kcal/mol for neutral clusters; (b)–(d) Relative cluster stability against atom addition for neutral, positively charged, and negatively charged clusters.

Since all the experimental spectra have structure with a period of four above $n = 10$, we have also investigated alternative graphitic structures corresponding to the well-known napthalene 1 and anthracene 2 aromatic molecules:

1 2

which could form by successive addition of four atoms to a benzene-like ring. However, the formation energies of the fully geometry-optimized structures was 130 and 250 kcal/mol higher, respectively, than for the corresponding monocyclic rings. This difference arises because of the strain present in the small six-membered rings.

The accuracy of the MNDO estimate of the strain energy was tested by computing the frequency of the C = C = C bending mode of allene. The force constant for this mode was used by Pitzer and co-workers[52,53] in an empirical estimate of the strain energy. The calculated frequency of 389 cm^{-1} is in good agreement with the measured value of 354 cm^{-1}.

In Figs. 3(b)–3(d) we show the scaled derivative defined in Eq. (13) for the neutral, positively charged, and negatively charged clusters. The peaks in this derivative correspond to structures most stable against atom addition. As is evident from the figure, this stability depends on the charge state. The most stable neutral clusters are at 10, 14, 18, and at 22–23, as discussed above. For the positively charged ones, however, the maxima are at 11, 15, 19, and 23. For negatively charged clusters, the chains are stable up to $n = 12$ and the maximum stabilities are at 14, 18, and 22.

C. Kinetics

In the reaction-limited regime, the scaled derivatives together with the differences between the entropies of the various structures determine the cluster stability in the laser vaporization source. The more stable clusters react less and show as maxima in the relative abundance spectra.

For carbon clusters, the scaled derivatives corresponding to the lowest energy structure [cf Figs. 3(b)–3(d)] were used together with a semiempirical value[52] of 20 cal/mol deg for the entropy difference between chains and rings. The coupled differential equations (3)–(6) were solved simultaneously for the neutral, the positively charged, and the negatively charged clusters. The starting conditions corresponded to a weakly ionized atomic vapor, with the concentration of the neutral atoms much greater than the concentration of ions. The variation of the catching radius R_{ij} with the cluster size in Eq. (15) was neglected.[57] The parameters α and γ were fitted to the spectra of the positive ions in the $n = 10$–23 range, because in this range all the

experiments show the same magic numbers. Good fits to spectra in the chain-ring crossover region around $n = 11$ required the average temperature $T_{av} \leqslant 500$ K. Although the adjustable temperature value is quite sensitive to the empirical value of the entropy difference between chains and rings, it still shows that the cooling in the source is very efficient. The value of ξ, which affects only the spectrum of the negative clusters, was determined from the distribution of negative clusters in the same range. In units in which the growth time is $t = 1$, the values of the parameters were[58] $x_1(t = 0)$ $\alpha = 4.5$, $\gamma = 0.02$, and $\xi = 0.1$.

The calculated spectrum of positive ions [Fig. 4(b)] should correspond most clearly to the experimental spectrum 2c labeled C_n^+. This is the spectrum of positive ions emerging directly from the source. The two spectra have the same overall shape, characteristic of aggregation kinetics. This shape is governed primarily by the parameter α. The magic numbers are determined by the exponential factor in Eq. (15). The parameter γ determines primarily the relative heights of the magic number peaks. The agreement between the calculated and the observed magic numbers is very good for $n \geqslant 10$, where both spectra show $4n + 3$ periodicity. The magic numbers at 11, 15, 19, and 23 are all well reproduced, as well as the relative intensity variations between the magic numbers.

In contrast to the range $10 < n < 25$, the range $n < 10$ appears to be very sensitive to experimental conditions, with magic numbers for these small clusters differing strongly for the positive ions shown in Fig. 2. One possible explanation for this behavior is that the small clusters are formed when the system is farthest from equilibrium and most sensitive to the technique used to evaporate the source. Thus flash evaporation might evaporate small clusters such as the rhombic structure for neutral C_4 which calculation of Pople and co-workers[51] have found to have nearly the same energy as the chain. A peak at C_3, on the other hand, may reflect a high concentration of photofragmentation secondaries.[9] For C evaporated in vacuum [the earliest data, Fig. 2(a)], a $\Delta n = 2$ periodicity is observed for both cations and anions, similar to the $\Delta n = 2$ periodicity which theoretical calculations (such as ours or Pitzer's) predict for neutral species. This periodicity has not been confirmed by more recent work, and it does not appear in our calculations for charged species (Fig. 3). It is possible that the apparently good agreement as regards $\Delta n = 2$ for $n < 10$ between theory and the early experimental work was accidental.

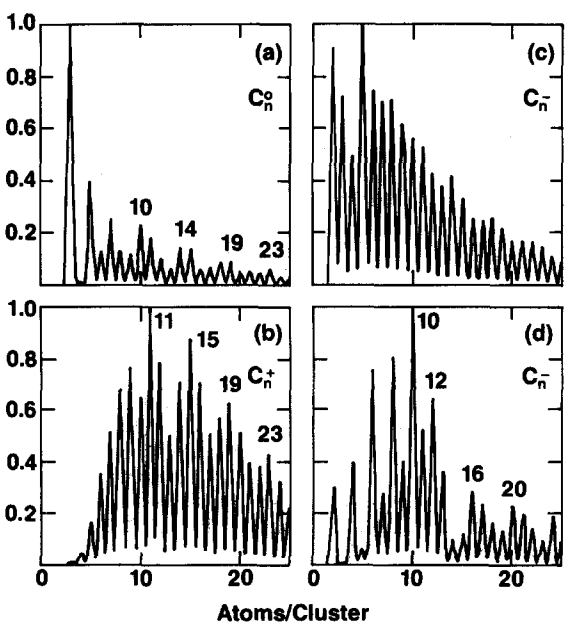

FIG. 4. Calculated relative abundances for (a) neutral clusters; (b) positively charged clusters; (c) negatively charged clusters without charge transfer effects; (d) negatively charged clusters with charge transfer effects.

The calculated distribution of neutral clusters [Fig. 4(a)] predicts the concentrations of clusters before photoionization. The calculated magic numbers for the neutral clusters are 10, 14, 18–19, and 22–23. A comparison to the spectrum of positive ions produced by photoionization of neutral clusters (labeled $C_n \rightarrow C_n^+$ in Fig. 3) shows that the experimentally measured distribution is strongly affected by the photoionization process. In particular, the experimental magic numbers at 11, 15, 19, and 23, corresponding to the series $4n + 3$, reflect more the stability of the charged rather than the neutral clusters. Moreover, photofragmentation branching studies have shown that C_3 is the most common photofragmentation product,[9] so that a number of $4n + 3$ clusters may be produced by a photoinduced ejection of C_3 fragments from stable $4(n + 1) + 2$ clusters. Other effects affecting the measured abundance spectrum are the photothreshold and photoionization cross section dependence on cluster size. The last effects are particularly important for carbon clusters in the $n = 1$–25 range, since these clusters are all multiphoton ionized.

The theoretical results for the negative ions calculated without the use of the charge transfer kernel [Eq. (16)] are shown in Fig. 4(c). These results compare very poorly with experimental distribution for the directly produced negative ions [Fig. 2(c)]. Allowing for the electron transfer between the negative ions and the neutral clusters brings the theoretical results [Fig. 4(d)] into good agreement with experiment. The overall shape of the experimental distribution is very well reproduced as well as the magic numbers at 10, 12, and 16. The magic cluster at 10 stands out because both its abundance among the neutrals and its electron affinity are high. The magic numbers at 18 and at 22, however, are not reproduced. A likely reason for this disagreement is the fact that the electron affinities for these large clusters are high, which inhibits electron transfer. The distribution of the largest negative ions would thus be determined more by the relative abundances of the neutral clusters than by the electron transfer effects. Indeed, the neutral cluster distribution has magic numbers at $n = 18$–19 and 22–23.

IV. SUMMARY AND CONCLUSIONS

We have developed a general, multicomponent kinetic model of cluster formation in the laser vaporization source. The model describes cluster growth via diffusion in the carrier gas. Both atom addition and cluster–cluster coagulation are important. Two limiting growth regimes exist, the *diffusion-controlled* regime, when the sticking probability is large

enough to assure cluster fusion during each encounter, and the *reaction-limited* regime, when many encounters are needed before cluster fusion takes place. In the diffusion-limited regime, the cluster distribution is essentially featureless. In the reaction-limited regime, the most stable clusters have the lowest probabilities for cluster fusion. This results in the increased abundance of these clusters in the cluster distribution, i.e., in the existence of magic cluster sizes.

The heat released in cluster formation allows small and medium size clusters to attain the energetically lowest or almost lowest atomic configurations. For larger clusters, the heat of fusion is insufficient to permit large scale atomic rearrangement. The uniqueness of structures of these clusters becomes strongly material dependent, for example, transition metal clusters are likely to form crystalline structures, while network-forming materials are likely to exibit a multitude of structures.

The kinetic equations for cluster growth are easily solved numerically, provided the aggregation kernel is known. For the reaction-limited regime, we have developed a consistent set of approximations which reduce the need for calculating the reaction probability for each pair of reacting clusters to the calculation of only the ground state energies of the clusters involved in aggregation. This is accomplished by the use of the Polanyi–Bronsted approximation and requires one adjustable parameter for the description of the aggregation process and one parameter for the description of the electron transfer process. The last parameter is needed only for calculation of the negative cluster distribution. The unknown vapor concentration is the only other adjustable parameter.

This formalism has been applied to carbon clusters in the $n = 1$–25 range. The structures of the clusters are determined by the requirement that the covalently bonded clusters have a minimum number of dangling bonds. Since carbon readily forms strong multiple bonds, the structures compatible with this requirement turn out to be π-bonded chains and monocyclic rings. A π-bonded ring is energetically lower only for the larger clusters, because bending of an *sp*-bonded chain introduces strain into the system.

We have carried out self-consistent MNDO calculations for the neutral clusters and for the positive and negative ions in both the chain and ring configurations. A limited number of other structural arrangements was geometry optimized and found energetically less favorable. For the neutral and for the positively charged clusters, the transition from chains to rings is predicted to occur at $n = 10$. This prediction has been partially verified to the experiments of Geusic *et al.*,[9] who see strong evidence for a structural transformation at $n = 10$ for positive ions. For the positive ions, rings continue to be the preferred structures above $n = 10$, while the $n = 11$–12 neutral clusters remain chains. For negative ions, the transition from chains to rings occurs at $n = 13$ according to our calculations.

The calculated formation energies together with a semiempirical estimate of the entropy difference between chains and rings were used as input in the kinetic calculations. The calculated cluster distributions are in good agreement with the experimental data for both the positive and the negative ions produced directly in the source. The magic numbers in the $n = 10$–25 range are also well reproduced. For the negative ions, it is found that the electron transfer effects have a strong effect on the measured distribution of small and medium size clusters. For the positive ions obtained via photoionization of neutral clusters, the calculated cluster distribution shows that the photofragmentation and/or photothreshold and photoionization cross section dependence on cluster size have a major effect on the measured spectra in the C_1–C_{25} range. For large clusters, however, the differences in stability between neutral and charged clusters should be smaller and the fragmentation energies should be larger. This may explain the dominance of C_{60} in *both* the positive and negative ion spectra, as observed recently by Smalley and co-workers.[59]

ACKNOWLEDGMENTS

It is a pleasure to thank D. M. Cox, A. Kaldor, D. J. Trevor, R. L. Whetten, T. A. Witten, and M. E. Geusic for several helpful discussions.

[1]T. G. Dietz, M. A. Duncan, D. E. Powers, and R. E. Smalley, J. Chem. Phys. **74**, 6511 (1981).
[2]V. E. Bondybey and J. H. English, J. Chem. Phys. **74**, 6978 (1981).
[3]D. E. Powers, S. G. Hansen, M. E. Geusic, A. C. Pulu, J. B. Hopkins, T. G. Dietz, M. A. Duncan, P. R. R. Langridge-Smith, and R. E. Smalley, J. Chem. Phys. **76**, 2556 (1982).
[4](a) E. A. Rohlfing, D. M. Cox, and A. Kaldor, J. Chem. Phys. **81**, 3322 (1984); (b) D. M. Cox, D. J. Trevor, and K. Reichmann, J. Am. Chem. Soc. (in press).
[5]M. E. Geusic, M. D. Morse, and R. E. Smalley, J. Chem. Phys. **82**, 590 (1985).
[6]R. L. Whetten, D. M. Cox, D. J. Trevor, and A. Kaldor, J. Phys. Chem. **89**, 566 (1985).
[7]R. L. Whetten, D. M. Cox, D. J. Trevor, and A. Kaldor, Phys. Rev. Lett. **54**, 1494 (1985).
[8]L. A. Bloomfield, R. R. Freeman, and W. L. Brown, Phys. Rev. Lett. **54**, 2246 (1985).
[9]M. E. Geusic, T. J. McIlrath, M. F. Jarrold, L. A. Bloomfield, R. R. Freeman, and W. L. Brown, J. Chem. Phys. **84**, 2421 (1986).
[10]L. A. Bloomfield, M. E. Geusic, R. R. Freeman, and W. L. Brown, Chem. Phys. Lett. **121**, 33 (1985).
[11]L.-S. Zheng, P. J. Brucat, C. L. Pettiette, S. Yang, and R. E. Smalley, J. Chem. Phys. (in press); P. J. Brucat, L.-S. Zheng, C. L. Pettiette, S. Yang, and R. E. Smalley, J. Chem. Phys. **84**, 3078 (1986).
[12]S. C. Richtsmeier, E. K. Parks, K. Lin, L. G. Pobo, and S. J. Riley, J. Chem. Phys. **82**, 3659 (1985).
[13]D. J. Trevor, D. M. Cox, K. Reichmann, and A. Kaldor, J. Phys. Chem. (submitted).
[14]S. C. O'Brien, Y. Liu, Q. Zhang, J. R. Heath, F. K. Tittel, R. F. Curl, and R. E. Smalley, J. Chem. Phys. **84**, 4074 (1986).
[15]D. J. Trevor, R. L. Whetten, D. M. Cox, and A. Kaldor, J. Chem. Soc. **107**, 518 (1985).
[16]J. C. Phillips, J. Non-Cryst. Solids **34**, 153 (1979); Phys. Status. Solidi B **101**, 473 (1980).
[17]N. Fürstenau and F. Hillenkamp, Int. J. Mass Spectrum. **37**, 155 (1981).
[18]R. J. Beuhler and L. Friedman, J. Chem. Phys. **77**, 2549 (1982).
[19]O. Echt, K. Sattler, and E. Recknagel, Phys. Rev. Lett. **47**, 1121 (1981).
[20]W. D. Knight, K. Clemenger, W. A. de Heer, W. A. Saunders, M. Y. Chou, and M. L. Cohen, Phys. Rev. Lett. **52**, 2141 (1984).
[21]J. R. Heath, Y. Lin, S. C. O'Brien, Q. L. Zhang, R. F. Curl, R. E. Smalley, and F. K. Tittel, J. Chem. Phys. **83**, 5520 (1985).
[22]H. W. Kroto, J. R. Heath, S. C. O'Brien, R. F. Curl, and R. E. Smalley, Nature **318**, 162 (1985); Q. L. Zhang, S. C. O'Brien, J. R. Heath, Y. Liu, R. F. Curl, H. W. Kroto, and R. E. Smalley, J. Chem. Phys. (to be published).
[23]J. C. Phillips, Chem. Rev. **86**, 619 (1986).

[24]J. J. Saenz, J. M. Soler, and N. Garcia, Surf. Sci. **156**, 121 (1985).
[25]H. Haberland, Surf. Sci. **156**, 305 (1985).
[26]D. Kreisle, O. Echt, M. Knapp, and E. Recknagel, Phys. Rev. B **33**, 768 (1986).
[27]M. Y. Chou, A. Cleland, and M. L. Cohen, Solid State Commun. **52**, 645 (1984).
[28]K. Clemenger, Phys. Rev. B **32**, 1359 (1985).
[29]J. Diefenbach and T. P. Martin, J. Chem. Phys. **83**, 4585 (1985), and references therein.
[30]O. F. Hagena, Surf. Sci. **106**, 101 (1981).
[31]J. M. Soler, N. Garcia, O. Echt, K. Sattler, and E. Recknagel, Phys. Rev. Lett. **49**, 1857 (1982).
[32]J. M. Soler and N. Garcia, Phys. Rev. A **27**, 3300 (1983).
[33]J. Bernholc and J. C. Phillips, Phys. Rev. B **33**, 7395 (1986).
[34]For graphite, which has a layer structure with weak interlayer bonding, it has been suggested that large pieces of graphitic sheets are also boiled of the surface (see Ref. 22).
[35]Since the photoionization thresholds of atoms and diatomics are in general higher than these of larger clusters, the relative abundances of atoms and diatomics are underestimated in the measured cluster distribution spectra.
[36]C. V. Heer, *Statistical Mechanics, Kinetic Theory and Stochastic Processes* (Academic, New York, 1972), p. 242.
[37]E. M. Lifshitz and L. P. Pitaevskii, *Physical Kinetics* (Pergamon, New York, 1981), p. 42.
[38]L. D. Landau and E. M. Lifshitz, *Fluid Mechanics* (Pergamon, New York, 1959), p. 228.
[39](a) Ph. Buffat and J-P. Borel, Phys. Rev. A **13**, 2287 (1976); (b) R. S. Berry, J. Jellinek, and G. Natanson, Phys. Rev. A **30**, 919 (1984); (c) S. Iijima and T. Ichihashi, Phys. Rev. Lett. **56**, 616 (1986); (d) P. A. Montano, G. K. Shenoy, E. E. Alp, W. Schulze, and J. Urban, Phys. Rev. Lett. **56**, 2076 (1986); (e) C. Herring, in *Structure and Properties of Solid Surfaces*, edited by R. Gomer and C. S. Smith (University of Chicago, Chicago, 1953), p. 5.
[40](a) T. A. Whitten and L. M. Sander, Phys. Rev. Lett. **47**, 1400 (1981); (b) M. Kolb and R. Julien, J. Phys. (Paris) Lett. **45**, L-977 (1984).
[41]A. Ourmazd, J. C. Bean, and J. C. Phillips, Phys. Rev. Lett. **55**, 1599 (1985).
[42]See S. Chandrasekkar, Rev. Mod. Phys. **15**, 1 (1943).
[43]J. M. Moore and R. G. Pearson, *Kinetics and Mechanism*, 3rd ed. (Wiley, New York, 1981), p. 240.
[44]Magic numbers in the mass spectra can also occur due to evaporation processes, see the preceding subsection.
[45]R. J. Cohen and G. B. Benedek, J. Chem. Phys. **86**, 3696 (1982).
[46]E. A. Moelwyn-Hughes, *Physical Chemistry* (Pergamon, New York, 1961), p. 1265. The catalytic reactions for which this relation has been used take place much closer to equilibrium, and the successful extrapolation to cluster aggregation is encouraging.
[47]R. E. Honig, J. Chem. Phys. **22**, 126 (1954).
[48]N. Fürstenau, F. Hillenkamp, and R. Nitsche, Int. J. Mass Spectrum **31**, 85 (1979).
[49]M. D. Newton and R. E. Stanton, J. Am. Chem. Soc. (submitted).
[50]J. March, *Advanced Organic Chemistry*, 2nd ed. (McGraw-Hill, New York, 1977), p. 28.
[51]R. A. Whiteside, K. Raghavachari, D. J. Defrees, J. A. Pople, and P. R. von Schleyer, Chem. Phys. Lett. **78**, 538 (1981).
[52]K. S. Pitzer and E. Clementi, J. Am. Chem. Soc. **81**, 4477 (1959).
[53]S. J. Strickler and K. S. Pitzer, in *Molecular Orbitals in Chemistry*, edited by B. Pullman and P. O. Löwdin (Academic, New York, 1964), p. 281.
[54]R. Hoffmann, Tetrahedron **22**, 521 (1966).
[55]M. J. S. Dewar and W. Thiel, J. Am. Chem. Soc. **99**, 4899 (1977); QCPE program No. 371.
[56]This was necessary because of the known tendency of semi-empirical calculations to predict alternating single and triple carbon–carbon bonds (see Ref. 55, and references therein). We found this unrealistically exaggerated tendency in some of our calculations for rings and for charged species and have decided to omit this effect. Some degree of bond alternation may, however, exist in these systems.
[57]The inclusion of a $(i^{1/3}+j^{1/3})^3$ factor into the aggregation kernel does not alter the quality of the fit in the $n = 1$–25 range and results only in a rescaling of the parameter α. For calculations over a wider range of cluster sizes the inclusion of the R_{ij} dependence on cluster size should be more significant.
[58]The results are invariant under the substitution $\hat{x}_i = \nu x_i$, $\hat{\alpha} = \alpha/\nu$.
[59]R. E. Smalley *et al.*, 191st ACS National Meeting, New York, 1986.
[60]G. D. Watkins and J. W. Corbett, Phys. Rev. A **134**, 1359 (1964).
[61]R. W. Baluffi, J. Nucl. Mater. **69/70**, 240 (1978).
[62]W. Wycisk and M. Feller-Kniepmeier, J. Nucl. Mater. **69/70**, 616 (1978).